Journal Name

ARTICLE

Simultaneous use of MOFs MIL-101(Cr) and ZIF-11 for Thin Film Nanocomposite Organic Solvent Nanofiltration

Carlos Echaide-Górriz[a], Marta Navarro[a], Carlos Téllez[a] and Joaquín Coronas[a,*]

Received 00th January 20xx,
Accepted 00th January 20xx

DOI: 10.1039/x0xx00000x

www.rsc.org/

MOFs Cr carboxilate MIL-101(Cr) and Zn imidazolate ZIF-11 have different chemical and textural properties. These properties have been combined to prepare thin film nanocomposite (TFN) membranes for organic solvent nanofiltration (OSN) with the two MOFs simultaneously embedded in the same membrane. The TFN membrane containing only ZIF-11 permeated faster than that with only MIL-101(Cr) when filtering sunset yellow (SY) (4.9 $L \cdot m^{-2} \cdot h^{-1} \cdot bar^{-1}$) and acridine orange (AO) (3.2 $L \cdot m^{-2} \cdot h^{-1} \cdot bar^{-1}$), although MIL-101(Cr) alone gave rise in both cases to better rejections (above 90%)). The combination of the two MOFs led to a versatile TFN membrane that showed an intermediate performance that improved the rejections given by the TFN membrane synthesized with ZIF-11 and the permeances corresponding to the TFN membrane synthesized with MIL-101(Cr). The effect of the temperature on the TFN membranes designed for this work has also been studied, obtaining apparent activation energies of 13.2 ± 2.1 and 8.3 ± 1.1 $kJ \cdot mol^{-1}$ for OSN of pure methanol and SY-methanol, respectively.

Introduction

Nanofiltration was first applied to water treatment in several industries where the rejected molecule sizes were between those in reverse osmosis and ultrafiltration processes.[1] Organic solvent nanofiltration (OSN) aims at separating molecules from specific organic solvents economically as well as efficiently. This requires the use of solvent-resistant membrane materials. It is worth mentioning that OSN has already been used in commercial organic solvent applications: e.g. in the production of the yellow pigment xanthophylls and in the Max-DewaxTM process for solvent lubricant dewaxing.[1]

In 1980, Cadotte et al. developed thin film composite membranes (TFC), improving some characteristics of previously existing membranes such as the membrane stability against several chemical species and the low permeation.[2] In 2007 Jeong et al. incorporated inorganic nanoparticles into the thin film, giving rise to the so-called thin film nanocomposite (TFN) membranes.[3]

Recently, Sorribas et al.,[4] Wang et al.[5] and Duan et al.[6] have modified TFC membranes with nanoporous crystalline metal-organic frameworks (MOFs) for nanofiltration purposes, whose organic-inorganic character allows strong and stable interactions between them and the thin film polymer (polyamide, PA). Besides, MOFs offer larger specific surface areas than zeolites, which have been shown to be a highly influential characteristic in the TFN membrane formed. Sorribas et al. tested MOFs ZIF-8, MIL-53(Al), NH_2-MIL-53(Al) and MIL-101(Cr) as fillers for TFN membranes, the latter being the nanostructure which generated the highest permeation while maintaining high rejection rates.[4] Importantly, Jimenez-Solomon et al. studied the mechanism that explains the influence of dimethylformamide (DMF) post-treatment on TFC membranes,[7] this being mainly the enhancement of the permeance through the dissolution of low molecular weight PA fragments because of the high compatibility with the DMF. Their conclusions were partly based on the studies carried out by Freger, among others, which led to the hypothesis about the stability of the PA thin film in DMF.[8, 9] Sorribas et al.[4] subsequently verified that such post-treatment was also efficient in the case of MOF-based TFN membranes and Echaide-Gorriz et al.[10] applied them to TFN-MOF membranes designed using MIL-68(Al) and ZIF-11 in addition to MIL-101(Cr) as nanosized fillers. These researchers studied a variety of PA syntheses, filtrating different types of solvents and solutes. They concluded that solvent-PA and solute-PA interactions, and the hydrophilicity of the TFN membrane, tuned by the presence of the corresponding filler, were the most influential parameters on the TFN membrane performance. Besides, other researchers such as Vankelecom et al.[11] have recently developed new synthesis methods of producing thin film nanocomposites for reverse osmosis applications. However, the use of other nanostructures is also being studied. For example, Wang et al.[12] have embedded graphene oxide and ZIF-8 in thin film composite membranes that proved useful for antimicrobial performance during separation processes.

In this work, two different types of nanosized MOFs have simultaneously been incorporated in the same TFN membrane for OSN application, and the performance of the resulted membrane has been compared with that of a TFC membrane and those of TFN membranes obtained with MIL-101(Cr) or ZIF-

[a] Chemical and Environmental Engineering Department and Instituto de Nanociencia de Aragón (INA), Universidad de Zaragoza, 50018 Zaragoza, Spain
† Corresponding author: coronas@unizar.es

Electronic Supplementary Information (ESI) available: Experimental details of particle synthesis, characterization of particles and membranes, detailed OSN results and temperature effect linear fit to Arrhenius Equation. See DOI: 10.1039/x0xx00000x

11 alone. A successful outcome has been obtained from the synergistic effects of both MOFs. MIL-101(Cr) is a hydrophilic carboxylate type MOF with 12-16 Å apertures connected to cages of 29 and 34 Å,[13] while ZIF-11 is a hydrophobic imidazolate type MOF with 14.6 Å pores connected through 3.0 Å appertures[14]. Both have already been used for OSN with good results.[4, 10] The resultant TFN membranes have been post-treated with DMF and tested with sunset yellow (450 Da) and acridine orange (260 Da) solutes to compare their expected distinct interaction with conventional TFN membranes. The TFN membrane operation was tested in a 6 h OSN process, where its performance and stability was periodically observed. Other researchers such as Sorribas et al.[4] and Jimenez-Solomon et al.[15] carried out this type of test, proving the membranes stability against several solvents (DMF, THF and methanol), what is of paramount importance from the point of view of the OSN industrial application. Besides, this is the first time that this type of MOF combination has been applied to TFN membranes. Previously, Zornoza et al.,[16] Valero et al.[17] and Jeazet et al.[18] combined nanoparticles of different nature to form MOF-based mixed matrix membranes for gas separation, also obtaining interesting results.

Moreover, in the field of aqueous nanofiltration through commercial polymeric membranes, the effect of temperature on the corresponding structure and process performance is a crucial parameter.[19, 20] A major goal in the removal of waste effluents containing organic colouring agents and other contaminants produced by several manufacturing industries is to study the OSN processes at relatively high temperature, especially in relation to the pulp, paper, sugar and textile industries.[19] A second novelty of this work corresponds to the study of the effect of temperature up to 55 °C in the OSN performance of TFN membranes. We report on their stability and high selectivity during the whole temperature cycle. Indeed, the effect of temperature was widely observed in nanofiltration and reverse osmosis processes of aqueous feeds.[19-21] Nevertheless, here we report for the first time the effect of temperature in a nanofiltration process of an organic feed, which consists of methanol and a dye.

Experimental

MOF synthesis

MIL-101(Cr) synthesis followed the improved method developed by Zhao et al.[22] based on the previous work by Khan et al.[23] Nanosized ZIF-11 was obtained following the synthesis described by Sanchez-Lainez et al.[24] The detailed synthesis procedures can be found in the Supporting Information.

Membrane synthesis

TFC and TFN membranes were prepared by interfacial polymerization (IP) of polyamide (PA) with 30 mL of a solution with 2% (w/v) of m-phenylenediamine (MPD) in water and 30 mL of a solution with 0.1% (w/v) of trimesoil chloride (TMC) and 0.2% (w/v) of dispersed MOF (if added) in hexane. When combining the MOFs, 0.1% (w/v) of MIL-101(Cr) and 0.1% (w/v) of ZIF-11 were simultaneously dispersed in the TMC hexane solution. The PA thin film was synthesized on a cross-linked asymmetric porous support of polyimide P84®. This support was obtained by the casting of a polymer dope solution of 24 wt% of P84® (HP polymer GmbH), dissolved in dimethylformamide (DMF – 99.5%, Scharlab), on polypropylene non-woven 40 cm x 40 cm sheet supports (Freudenberg). The phase inversion took place at 23 °C in distilled water as the non-solvent. The cast asymmetric supports were finally treated with hexanediamine (HDA – 98%, Sigma Aldrich) and polyethylene glycol (PEG – synthesis grade, Scharlab) separately. They were cross-linked with hexanediamine, so that they became stable in organic solvents. A final treatment with polyethylene glycol avoided pore collapse during the interfacial polymerization,[4] and allowed a better control of the PA thin film formation.[25] With the purpose of a complete comparison, four different types of membranes were fabricated (Table 1): TFC membranes, and TFN membranes containing MIL-101(Cr) (TFNMIL101), ZIF-11 (TFNZIF11) and both MIL-101(Cr) and ZIF-11 (TFNMIL101-ZIF11).

Membrane	Aqueous phase	Organic phase (in hexane)
TFC	2% (w/v) MPD	0.1% (w/v) TMC
TFNZIF11	2% (w/v) MPD	0.1% (w/v) TMC + 0.2% (wt) ZIF11
TFNMIL101	2% (w/v) MPD	0.1% (w/v) TMC + 0.2% (w/v) MIL-101(Cr)
TFNMIL101-ZIF11	2% (w/v) MPD	0.1% (wt) TMC + 0.1% (w/v) MIL-101(Cr) + 0.1% (w/v) ZIF11

Table 1. Synthesis parameters for each type of membrane

As shown in other works,[4, 10] chemical post-treatments with DMF leads to improvements in the performance of both TFC and TFN membranes. Thus, 10 min DMF bathing at 20 °C was performed for all the membranes tested, while 10 min DMF filtration at 20 °C and 20 bar was only carried out for the TFN membranes with both MOFs combined.

MOF and membrane characterization

The size, morphology and intergrowth of the MOF crystals were checked using a scanning electron microscope (SEM) FEI-20 Inspect, operating at 10-20 kV. Transmission electron microscopy (TEM) images of the MOF crystals were taken using a FEI Tecnai T20, operated at 200 kV. X-ray diffraction analysis (XRD) was applied using a D-Max 2500 Rigaku X-ray diffractometer with a copper rotating anode operating at 40 kV and 80 mA at a wavelength of 1.5418 Å. A Mettler Toledo DSC-1 Star System was used to carry out the thermogravimetric analysis (TGA) at a heating rate of 10 °C·min^{-1} up to 700 °C, using air as gas. N_2 adsorption was carried out at -195 °C with a Micromeritics Tristar 300, outgassing at 200 °C during 8 h. The specific surface area was calculated through the Brunauer-Emmet-Teller method, while the pore volume was obtained by taking the adsorbed volume at a relative pressure of 0.98.

The membrane samples were characterized by contact angle measurement with a Krüss DSA 10 MK2 at 20 °C. SEM and

TEM were carried out under the same conditions as for the MOF characterization. A fragment of the PA film combined with ZIF-11 and MIL-101(Cr), detached from the polyimide support while the PA film was formed by interfacial polymerization, was placed onto a holey carbon grid. It was allowed to dry at ambient conditions and analysed by TEM to examine the presence, distribution and morphology of the two different MOF particles within the TFN membranes. STEM imaging and EDS analysis were performed using a FEI™ Tecnai G2 F30 microscope at 300 kV, to confirm the presence of Cr-MOF (MIL-101(Cr)) and Zn-MOF (ZIF-11) in the TFN membrane. Similarly, energy-dispersive X-ray microscopy (EDX) was used to estimate the concentration of the Cr and Zn atoms inside the PA thin film, and to study their distribution over the surface.

For characterization purposes, the IP of PA, with or without MOFs, was also carried out without the presence of the P84® support, at the same synthesis conditions than in the TFC and TFN membranes. Four samples, the pristine PA, the PA combined with MIL-101(Cr), the PA combined with ZIF-11 and the PA combined with both MOFs (added in a 50/50 weight proportion) were analysed by TGA. The goal of this analysis was to prove the presence of the MOFs by detecting the degradation of each component (PA and MOFs).

OSN measurement

Each membrane was measured in a dead-end nanofiltration module (Sterlitech HP4750) at 19 °C and 20 bar of feed pressure. The feed consisted of a 250 mL solution of 20 $mg \cdot L^{-1}$ of the solute in methanol. This solution was filtered through a 12 cm^2 membrane located at the bottom of the module. The influence of filtering two different solutes was studied with the above-mentioned four membrane types. The solutes were sunset yellow (SY, 450 Da – Sigma-Aldrich, 90% dye content) and acridine orange (AO, 260 Da – Acros Organics, 55% dye content).

The permeance and rejection were both calculated at the end of the filtration procedure with the equations already used by Echaide-Gorriz et al.[10] Concentrations of both permeate and residue were measured by an UV spectrometer (Jasco V-670 spectrophotometer), using water as solvent. For this purpose, after 30 min, the time needed for the process to stabilize, 3 mL aliquots of each permeate and residue were taken as samples for analysis. The methanol in the samples was allowed to evaporate and was replaced by 3 mL of deionized water at room temperature and pressure in order to be measured with the UV spectrometer. Absorbance and concentration values for each solute were determined using the appropriate calibration curve. Wavelengths of maximum absorbances of SY and AO were 480 and 291 nm, respectively. An extra performance test was carried out to observe the membrane operation stability. This test took 6 h, the feed consisted of methanol and SY and every 90 min it was replaced by a fresh solution.

Effect of the temperature

TFN membranes synthesized by the combination of MOFs MIL-101(Cr) and ZIF-11, post-treated by DMF filtration, were tested filtering SY in methanol at 19, 25, 40 and 55 °C. The temperature increased gradually and finally the performance was measured again at the starting temperature. The whole module was immersed in a water bath heated at the desired temperature and left to stabilize for at least 60 min before filtration, so that steady state was reached. This process was repeated with two membranes for reliability assessment. The same procedure was carried out in clean membranes synthesized in the same conditions but feeding pure methanol in order to test the membrane performance with temperature while avoiding the fouling effect of the solute.

Results and discussion

MOF and membrane characterization

SEM and TEM images showed similar crystal morphologies to those described in the literature for each MOF (see Figs. 1A, 1a, 1B, 1b).[22, 24] The average particle sizes were 173 ± 15 nm and 79 ± 10 nm for MIL-101(Cr) and ZIF-11, respectively, suitable for a good interaction with the polymer in the TFN membranes. It is worth mentioning that nanosized ZIF-11 was not crystalline like typical microsized crystals of the same MOF, as the XRD analysis showed (Fig. S1A of Supporting Information); however, most of the chemical and adsorption features of ZIF-11 can also be found in nanosized ZIF-11.[24] MIL-101(Cr) crystallinity was confirmed by XRD analysis (Fig. S1B of Supporting Information). TGA (Fig. S1C and S1D of Supporting Information) indicated that the solvent and unreacted linkers were washed out after the whole synthesis processes, i.e. the MOF nanoparticles were correctly activated. The BET specific surface area and pore volume of MIL-101(Cr) were 2139 $m^2 \cdot g^{-1}$ and 1.8 $cm^3 \cdot g^{-1}$, respectively. In the case of ZIF-11, the specific surface area could not be measured by nitrogen adsorption due to its narrow porosity; however, a CO_2 pore volume of 0.11 $cm^3 \cdot g^{-1}$ has been reported elsewhere for the material.[24]

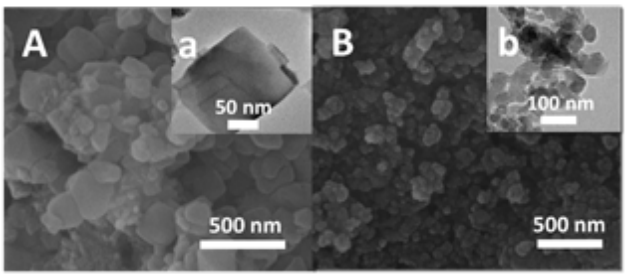

Fig. 1. SEM images of MIL-101(Cr) (A) and ZIF-11 (B), with insets showing TEM images of both MOFs (a and b).

Both Cr and Zn atoms, related to MIL-101(Cr) and ZIF-11, respectively, were detected by EDS analysis in a TFN membrane sample prepared with both MOFs (Fig. 2A). Three different zones of analysis were explored, as shown in Fig. 2A (together with the quantification results in Fig. 2B): zone 1 corresponds to an area where only Zn metal was detected, confirming the presence of ZIF-11; zone 2 reveals the presence of Cr alone, due

to the MIL-101(Cr); finally, zone 3 shows the presence of both Zn and Cr.

The presence of ZIF-11 in the TFN membrane is barely observable in the PA thin film prepared *ad hoc* for TEM observation (Fig. 2C and 2c). This is partly because of its small particle size and non-defined shape (see Fig. 1b), similar to the appearance of PA. Duan et al.[6] have studied the synthesis mechanism of TFN membranes with nanosized ZIF-8, basing their conclusions on the so-called template effect hypothesis first introduced by Lind et al. for TFN membranes prepared with nanocrystals of the LTA-type zeolite.[26] Both studies suggest that nanoparticles with sizes below the PA thin film thickness, as in the case of ZIF-11 (79 nm as compared to 100-150 nm of PA film thickness),[4, 27] tended to be fully surrounded by PA. This is another reason to explain why in Fig. 1D, ZIF-11 would not be as easily observable as MIL-101(Cr).

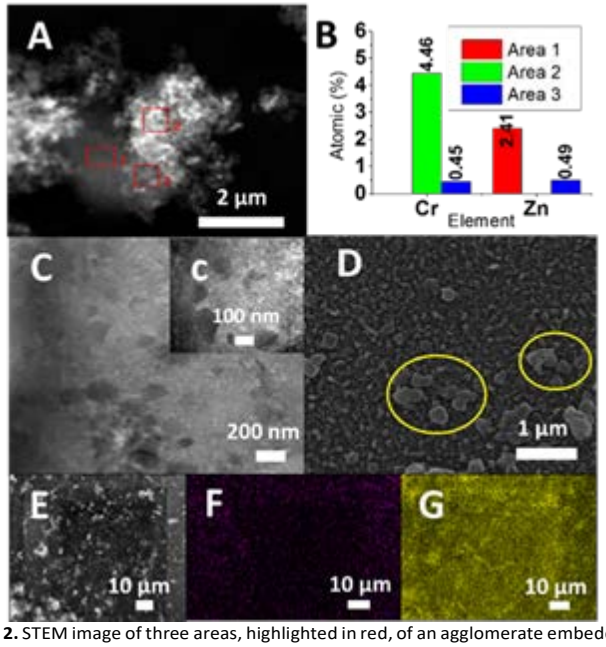

Fig. 2. STEM image of three areas, highlighted in red, of an agglomerate embedded in the PA thin film that belongs to a TFN membrane synthesized with both MOFs (A). Element quantification of the areas 1, 2 and 3 highlighted in red in image A (B). TEM image of PA thin film with embedded MOFs (C and inset c). SEM image of MIL-101(Cr) (highlighted with yellow circles) on the surface of the PA thin film, evidenced by the presence of ring-like structures (D). EDX mapping of Zn and Cr content (E and F). SEM image of the detached thin film (G).

EDX analysis showed the presence of both Zn and Cr in the area shown in Fig. 2E highly dispersed in the TFN membrane, once more related to MOFs ZIF-11 and MIL-101(Cr), respectively (Fig. 2F and 2G, see quantification in Table S1). Due to their larger particle size (around 173 nm, in principle greater than the PA film thickness of ca. 100 nm[4]), MIL-101(Cr) crystals protruded and were easily observed by SEM on the TFN membrane surface, while the smaller, round shaped particles of ZIF-11, probably embedded in the PA film, were not visible to the naked eye (Fig. 2D).

As previously reported, when a MOF is embedded in a polymer matrix, the MOF degradation temperature tend to increase.[28] This phenomena was observed when analysing the samples of MIL-101(Cr)-PA and ZIF-11-PA by TGA (Fig. 3 shows the corresponding derivative curves), corresponding to non-supported MOF-PA nanocomposites prepared *ad hoc*. These curves show that the MOF degradation took place at higher temperatures (374 and 595 ºC for MIL-101(Cr)-PA and ZIF-11-PA, respectively) than when the MOFs were considered alone (357 and 558 ºC for MIL-101(Cr) and ZIF-11, respectively, as shown in Figs. S1D and S1C). Interestingly, the PA degradation temperature changed in both cases: the degradation temperature of PA alone was 556 ºC, whereas in the presence of MIL-101(Cr) and ZIF-11 decreased to 441 and 518 ºC, respectively. As Cacho-Bailo et al.[28] previously observed in the particular case of the ZIF-8 embedded in polysulfone, the polymer degradation temperature decreased by around 90 ºC, depending on the MOF morphology and composite proportion. The reason for this was related to the Zn catalytic effect.[29] This effect is highly intensified when the MOF is already degraded and the metal is in its oxidized state, as proved by Zamaro et al.[30] in the case of HKUST-1. The same effect can be observed in the case of the Cr from MIL-101(Cr), which would be already oxidized when the PA started to degrade. In agreement with this observation, several authors have studied the functionalization of MIL-101(Cr) for catalysis applications,[31] as well as the catalytic effect of chromium terephthalate crystals for selective oxidation processes.[32] The high interest of many researchers in MIL-101(Cr) lays on its high porosity, efficient transport properties and high number of active sites.[33]

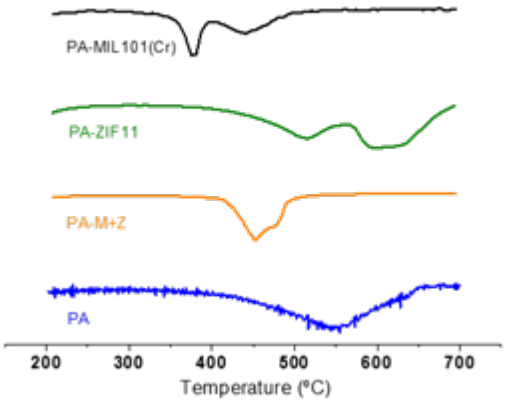

Fig. 3. Normalized TGA derivatives (DTG) of PA in blue, composite PA-M+Z (MIL-101(Cr) + ZIF-11) in orange, PA-ZIF-11 composite in green and PA-MIL101(Cr) in black.

The last sample analysed, which consisted of PA with both MOFs embedded, did not show any of the degradation temperatures corresponding to MIL-101(Cr)-PA or ZIF-11-PA. The only band was observed between 408 and 495 ºC (see Fig. 3), which may be the combination of two bands. This single band would have been obtained from the merge of the catalytic effects of the MIL-101(Cr) and ZIF-11, since the band appears at an intermediate temperature between the degradation temperatures of MIL-101(Cr)-PA and ZIF-11-PA. This combined band confirms the presence of both MOFs in the same composite.

The content of MOFs was also estimated in these non-supported MOF-PA nanocomposites. As can be seen in Table S2, the theoretical MOF content in every sample calculated from the initial synthesis parameters, considering a feasible displacement of the equilibrium reaction towards the products, was 61.2 wt%. The contents of MOFs in the samples estimated from the rests obtained after the corresponding TGA analyses are 73.7, 29.0 and 46.1 wt% for the PA composites containing MIL-101(Cr), ZIF-11 and the mixture of both. The content difference between the embedded MOFs, previously observed in the case of TFN membranes,[10] can be justified by the different chemical character of both (see the contact angles of the membranes synthesized in Table S4). The MIL-101(Cr) hydrophilicity intensifies the MOF interactions with the aqueous phase, rather than with the organic phase (hexane). As the MOF was dispersed in the organic phase, it tended to migrate to the aqueous phase when the reaction starts, ending up at the interface (where the reaction takes place). Consequently, the final proportion of MIL-101(Cr) in the sample was relatively high. On the contrary, ZIF-11 hydrophobicity enhances its interactions with the hexane. These interactions may decrease the amount of ZIF-11 in the interface, decreasing its final content in the sample, and giving rise to an intermediate value for the mixture of MOFs, as a result of their opposite chemical character.

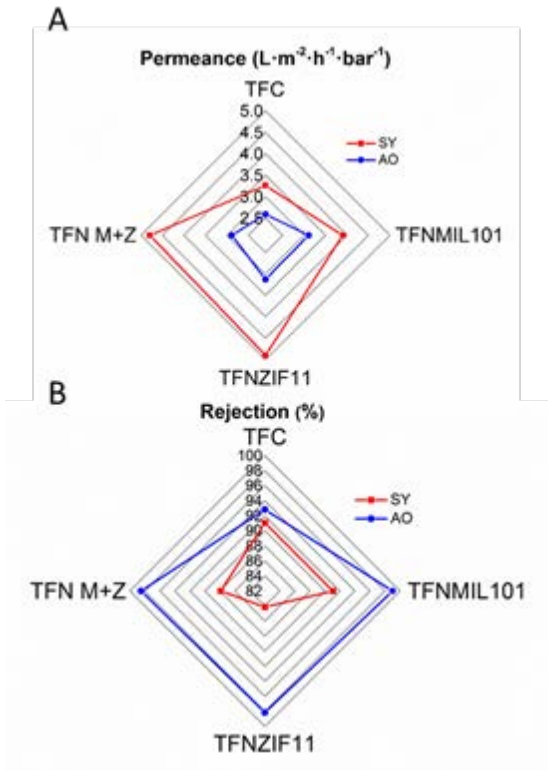

Fig. 4. Permeance of methanol (A) and rejection of solutes (B) for the membranes prepared. Blue and red polygons correspond to AO (260 Da) and SY (450 Da) OSN, respectively. TFN M+Z corresponds to the membrane with MIL-101(Cr) and ZIF-11 embedded. Values are averages of results obtained from at least two different membranes treated with the DMF bath and tested at 19 °C and 20 bar of feed pressure (see Table S3 with available errors).

OSN measurement

As show in Fig. 4A, all the three MOF-based TFN membranes achieve higher methanol permeances than the TFC membrane with eiher of the two dyes (AO and SY). In OSN of AO (260 Da) produced lower permeances than that of SY (450 Da), which suggests the diffusion of the smaller dye through the membrane giving rise to some fouling for methanol transport. The fouling phenomenon can be evaluated in terms of Hansen solubility parameters (HSP).[27, 34, 35] These parameters are δ_D, δ_P and δ_H for dispersion or London interaction, polar interaction and hydrogen bonds, respectively.

Table 2. HSP of acridine orange (AO), sunset yellow (SY) and polyamide (PA). Ra calculated taking PA HSP as reference.

	δ_D (MPa$^{0.5}$)	δ_P (MPa$^{0.5}$)	δ_H (MPa$^{0.5}$)	Ra (MPa$^{0.5}$)[a]
AO	20.2	3.2	6.4	9.9
SY	23.1	17.8	24.1	20.0
PA	18.0	11.9	7.9	0

[a] Calculated according to $Ra^2=4(\delta_{D1}-\delta_{D2})^2+(\delta_{P1}-\delta_{P2})^2+(\delta_{H1}-\delta_{H2})^2$ where δ_{D1}, δ_{P1} and δ_{H1} and δ_{D2}, δ_{P2} and δ_{H2} are the sets of parameters corresponding to AO or SY (1) and PA (2), respectively.

The comparison between the HSP of the PA and the solutes in terms of the calculation of the parameter Ra (see Table 3) means that they may have a mutual interaction in the following terms: the smaller the Ra value, the better the interaction. The Ra values are 9.9 and 20 MPa$^{0.5}$ for agreement with the above-mentioned lower methanol permeances in the presence of AO.

Fig. 4A and Table S3 reveal how the combination of MOFs resulted in a high permeance when filtering SY (4.8 L·m^{-2}·h^{-1}·bar^{-1}), very similar to the permeance flux obtained for the TFN membrane synthesized with only ZIF-11 as filler (4.9 L·m^{-2}·h^{-1}·bar^{-1}), and significantly higher than that shown by the TFN membrane with only MIL-101(Cr) (3.9 L·m^{-2}·h^{-1}·bar^{-1}). In contrast, as depicted in Fig. 4B and in Table S3, the rejection obtained with the TFNMIL101-ZIF11 membrane (87.9%) was higher than that obtained for the TFNZIF11 membrane (84.1%) but lower than that obtained for the TFNMIL101 membrane (91.1%). When filtering AO, the methanol permeance obtained was higher for the TFN membranes synthesized with only one MOF as filler, being 3.1 L·m^{-2}·h^{-1}·bar^{-1} for TFNMIL101 and TFNZIF11, see Fig. 4A and Table S3. However, as shown in Fig. 4B and Table S3, the TFN membrane synthesized with both MOFs combined (98.5%) showed a rejection slightly higher than that of the TFNZIF11 membrane (98.1%), together with lower standard deviation values (2.6 and 5.7% respectively, see Table S3), which is consistent with better membrane reproducibility. The TFN membrane synthesized with only MIL-101(Cr) showed a slightly higher rejection than the others (99.0 %). The TFNMIL101-ZIF11 membrane improved the rejection of SY and AO in comparison with the rejection measured for the TFNZIF11 membrane while maintaining a permeance flux similar to that of the latter. The TFN membrane synthesized with only MIL-101(Cr) showed a better performance when filtering AO than the TFNMIL101-ZIF11, but its methanol permeance when

filtering SY was significantly lower than that of either of the other two TFN membranes.

According to Sorribas et al.,[4] MIL-101(Cr) would lead to a TFN membrane with the highest solvent (methanol and THF) permeance. Moreover, it has been stated here that ZIF-11 contributes to higher permeances in OSN TFN membranes compared with MIL-101(Cr) alone, although with lower rejections. The role of both MOFs is complementary. On the one hand, the high specific surface area given by the MIL-101(Cr) contributes to the increase of permeance, although its hydrophilicity, as Sorribas et al.[4] mentioned, tends to reduce the flow of methanol. On the other, the ZIF-11 hydrophobicity causes the opposite effect,[10] by countering MIL-101(Cr) hydrophilicity. This effect, combined with the fact that ZIF-11 can also modify the PA cross-linking creating a more permeable thin layer, can explain the influence of this MOF on the TFN membrane performance.[6, 10] The diffusion of methanol through ZIF-11 pores, in spite of their small apertures, can also be possible. In this way, Park et al.[14] mentioned that ZIF-11 can allow the diffusion of N,N-diethylformamide molecules trapped in its 14.6 Å cavities. In recent studies, He et al.[36] have claimed that phenyl groups of the ZIF-11 ligand may swing to allow the entrance and exit of guest molecules without destroying the structure. This suggests that larger molecules than the ZIF-11 apertures (3.0 Å) may diffuse through its pores, as was observed in the case of ZIF-8 crystals by the so-called gate-opening effect,[37] when encapsulating and releasing caffeine.[38] Besides, Zhu et al.[39] have recently observed the presence of intercrystalline voids of 8.3 Å between aggregated ZIF-8 crystals.

The different surface chemistry of both MOFs (hydrophobic ZIF-11 and hydrophilic MIL-101(Cr)), affecting the contact angles of the membranes (e.g. the contact angle was 57º for the membrane obtained with MIL-101(Cr) alone, while it was 71-72º for the other three types of membranes – see Table S4), would enhance the filler dispersion in the TFN membrane, probably reducing the filler agglomeration and creating more MOF-polymer interfaces in which the solvent transport is promoted with some loss of selectivity. Consequently, the simultaneous use of MIL-101(Cr) and ZIF-11 in TFN membranes is of great interest, since it combines high permeance and rejection related to MOFs ZIF-11 and MIL-101(Cr), respectively.

Effect of the post-treatment

The permeance flow was greatly enhanced (see Fig. 5) for both SY and AO solutes when the membrane was post-treated with DMF filtration instead of the DMF bath. The similarity between PA and DMF HSP, giving rise to a Ra value of 4.0,[10] explains the DMF influence on the membrane in agreement with the behaviour reported by Jimenez-Solomon et al.[7] The increase in permeance is explained by a decrease in the transport resistance due to the removal of low molecular weight PA polymer fragments. When the DMF bath is applied to a membrane, only the superficial fragments of the PA thin film are removed, while when the DMF filtration is carried out the dissolution affects the bulk PA layer.

When filtering the membrane with DMF, SY rejection increased; however, AO rejection decreased. As reported

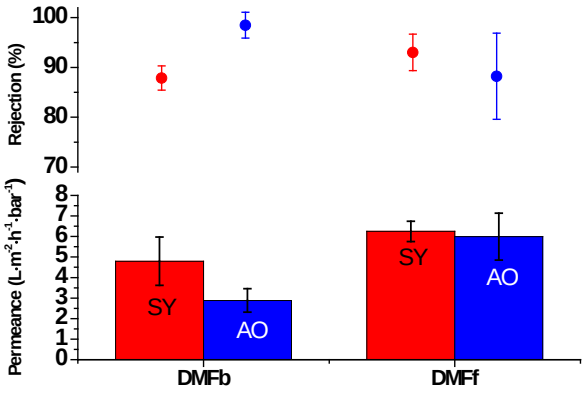

Fig. 5. Effect of post-treatment applied to a membrane synthesized with both MOFs MIL-101(Cr) and ZIF-11 combined. DMFb stands for DMF bath and DMFf for DMF filtration. Red represents results obtained when filtering methanol with SY and blue when filtering methanol with AO. Conditions: 19 ºC and 20 bar of feed pressure.

elsewhere,[10] three different mechanisms can explain the changes in solute rejection (namely a swelling effect provoked in the membrane when in contact with DMF, a healing process of a defect on the surface by surface tension driven pore collapse and the dissolution of PA monomers during the DMF filtration treatment rejected by the PA thin film), all of them giving rise to the healing of the thin selective film. These mechanisms probably worked for the SY due to its relatively large size, although they were not applicable to the AO because it was too small to be rejected by the healed spaces.

The physical consequences of the post-treatment on the PA thin film are not easily evidenced through SEM characterization.[7] Here, some differences were observed when comparing the SEM images (see Fig. S2) corresponding to membranes with no post-treatment and treated with DMF filtration (the most aggressive of the two applied in this work). The PA ring-like shapes, which appear as a consequence of the IP,[25] lose their well-defined shape after the chemical treatment.[7] As mentioned in different works,[4, 7, 9, 10] only low molecular mass PA fragments, located at the top and bottom surfaces to the film, can be dissolved by the DMF, since, as Freger mentioned,[8] the PA thin film core would keep unmodified.

Besides the 50/50, two additional weight proportions of MIL-101(Cr) and ZIF-11 were embedded into TFN membranes, keeping constant the total amount of filler: 25/75 and 75/25 ZIF-11/MIL-101(Cr). These membranes were treated with DMF filtration and tested with the feed of methanol and SY (see Fig. S3). No regular tendency was observed within the experimental error, the MOFs having a qualitative effect with no dependence on the ZIF-11/MIL-101(Cr) relative content, in the range of conditions tested.

Influence of the operation time

Although in a dead-end module, the permeance will never reach a stationary regime, a stable flow was usually achieved after 2 h of operation (see Fig. S4 for a TFC membrane). Since the TFC membrane

performance was measured in a dead-end module, every 90 min the membrane module had to be opened and refilled with fresh SY-methanol feed solution. In that moment, the pressure inside the module dropped to room pressure, provoking the observed fluctuations (Fig. S4). Other researchers such as Jimenez-Solomon et al. observed the effect of DMF filtration during 200 h in a cross-flow installation with analogous PA based membranes.[7]

Effect of the temperature

Fig. 6 illustrates how the permeance increased with temperature. Two important observations should be made at this point: the methanol permeance increased with temperature in the whole range studied, and the permeance at 19 °C was lower after the heating cycle than at the beginning of the run.

The first observation can be explained by the influence of temperature on the permeating fluid viscosity and the diffusion mechanism through the membrane pores. As He et al.[21] suggested, the increase in solvent permeance can be explained by the effect of temperature on the dye solution viscosity. The dependence of the diffusion coefficient and the transport resistance on the viscosity supports this hypothesis. Besides, in the cited work, this parameter was measured at the feeding point at different temperatures in order to observe such dependence. In addition to this effect, as the temperature increases, less solute and solvent is physically adsorbed on the membrane surface. Their mobility therefore increases and the activated transport through the filler micropores also increases.[40] Importantly, the membrane fouling decreases due to the lower adsorption of solute molecules on the membrane surface, contributing to the decrease in the transport resistance.[1] However, the fouling phenomenon still takes place; even though the temperature is relatively high. The methanol permeance when pure methanol was fed was higher than that when the dye solution was fed at any temperature (see Fig. 6).

The methanol permeance drop after the heating cycle gave rise to a hysteresis (see Fig. 6). Mänttäri et al.[19] distinguished between two possible contributions to explain the changes that a membrane experiences after being heated to a relatively high temperature during the OSN process. They suggested that the fouling phenomenon influences the membrane performance, due to a solute adsorption increase. They also mentioned that a modification to the membrane structure can occur depending on the membrane material.[19] This phenomenon was previously studied by Yao et al.[41], who did not observe any irreversible changes in the structure of membranes synthesized with a certain proportion of polyethersulfone and polyvinylpyrrolidone and applied to the pre-treatment of Kraft Pulp Bleach. However, they reported an irreversible pore diameter dilatation when the mixture of the above- mentioned polymers was modified. In contrast, solute rejection did not significantly change with the temperature, although it slightly increased when the membrane cooled down and was measured again at 19 °C (Fig. 6). This phenomenon can be explained by the membrane fouling or irreversible compression of the PA thin film.

Fig. S5 depicts the Arrhenius plot of ln (P_T/P_{T0}) as a function of 1/T (where P_T and P_{T0} are the permeances in $L \cdot m^{-2} \cdot h^{-1} \cdot bar^{-1}$ at T and 19 °C, respectively, and T is the temperature in K), which shows that the apparent activation energy was higher when permeating pure methanol than when SY was dissolved in methanol: 13.2 ± 2.1 and 8.3 ± 1.1 $kJ \cdot mol^{-1}$, respectively. This difference might be related to the absence of SY, which would interact with the membrane, as mentioned above, particularly with the filler microporosity promoting a less activated flow. This is consistent with the hypothesis that the filler microporosity would contribute to a more activated flow, as claimed for zeolites.[40] On the other hand, the possible interactions between solute and solvent cannot be discarded. All these interactions make it difficult to interpret the transport mechanism through the membrane. In any event, the permeance is clearly favoured with temperature, which is of interest when dealing with the industrial application of OSN.

Fig. 6. Effect of temperature on TFNMIL101-ZIF11 membrane, having both ZIF-11 and MIL-101(Cr) fillers. The values in black squares represent the results when filtrating methanol with SY, while the values in orange circles represent the results when filtrating pure methanol. The values that do not belong to the lines drawn correspond to the measurements obtained after the temperature cycle.

Conclusions

The composites and membranes synthesized embedding simultaneously two different MOFs (ZIF-11 and MIL-101 (Cr) as fillers showed synergistic effects, combining the hydrophobicity of the ZIF-11 and the hydrophilicity and high porosity of the MIL-101(Cr). Consequently, the combination of both MOFs led to an enhanced and versatile membrane, whose performance was even further improved when DMF postreatments were applied. This strategy could be applied to other pairs of MOFs to optimize the separation performance of nanofiltration systems including different solvents and solutes.

The temperature influenced the performance of the TFN membranes synthesized by reducing the feed viscosity and by reducing the solute adsorption on the structure of the membrane. Interestingly, the effect of the temperature resulted irreversible, since the permeance of methanol decreased when the temperature returned to the initial temperature. However, the solute rejection remained unchanged.

Acknowledgements

Financial support (MAT2013-40556-R, MAT2016-77290-R) from the Spanish MINECO, the Aragón Government (DGA, T05), the European Social Fund and FEDER is gratefully acknowledged. We also acknowledge the use of the Servicio General de Apoyo a la Investigación-SAI (Universidad de Zaragoza). All the microscopy work was done in the Laboratorio de Microscopías Avanzadas at the Instituto de Nanociencia de Aragón (LMA-INA). The authors acknowledge the LMA-INA for offering access to their instruments and expertise. Prof. Dr. Steven Abbott is thanked for providing Hansen solubility parameters.

Notes and references

1. P. Vandezande, L. E. M. Gevers and I. F. J. Vankelecom, *Chem. Soc. Rev.*, 2008, **37**, 365-405.
2. J. E. Cadotte, R. J. Petersen, R. E. Larson and E. E. Erickson, *Desalination*, 1980, **32**, 25-31.
3. B. H. Jeong, E. M. V. Hoek, Y. S. Yan, A. Subramani, X. F. Huang, G. Hurwitz, A. K. Ghosh and A. Jawor, *J. Membr. Sci.*, 2007, **294**, 1-7.
4. S. Sorribas, P. Gorgojo, C. Tellez, J. Coronas and A. G. Livingston, *J. Am. Chem. Soc.*, 2013, **135**, 15201-15208.
5. L. Y. Wang, M. Q. Fang, J. Liu, J. He, J. D. Li and J. D. Lei, *ACS Appl. Mater. Interfaces*, 2015, **7**, 24082-24093.
6. J. T. Duan, Y. C. Pan, F. Pacheco, E. Litwiller, Z. P. Lai and I. Pinnau, *J. Membr. Sci.*, 2015, **476**, 303-310.
7. M. F. J. Solomon, Y. Bhole and A. G. Livingston, *J. Membr. Sci.*, 2012, **423**, 371-382.
8. V. Freger, *Langmuir*, 2003, **19**, 4791-4797.
9. V. Freger, *Environm. Sci. Technol.*, 2004, **38**, 3168-3175.
10. C. Echaide-Górriz, S. Sorribas, C. Téllez and J. Coronas, *RSC Adv.*, 2016, **6**, 90417-90426.
11. C. Van Goethem, R. Verbeke, S. Hermans, R. Bernstein and I. F. J. Vankelecom, *J. Mater. Chem. A*, 2016, **4**, 16368-16376.
12. J. Wang, Y. M. Wang, Y. T. Zhang, A. Uliana, J. Y. Zhu, J. D. Liu and B. Van der Bruggen, *ACS Appl. Mater. Interfaces*, 2016, **8**, 25508-25519.
13. G. Ferey, C. Mellot-Draznieks, C. Serre, F. Millange, J. Dutour, S. Surble and I. Margiolaki, *Science*, 2005, **309**, 2040-2042.
14. K. S. Park, Z. Ni, A. P. Cote, J. Y. Choi, R. D. Huang, F. J. Uribe-Romo, H. K. Chae, M. O'Keeffe and O. M. Yaghi, *Proc. Natl. Acad. Sci. U. S. A.*, 2006, **103**, 10186-10191.
15. M. F. Jimenez-Solomon, P. Gorgojo, M. Munoz-Ibanez and A. G. Livingston, *J. Membr. Sci.*, 2013, **448**, 102-113.
16. B. Zornoza, B. Seoane, J. M. Zamaro, C. Tellez and J. Coronas, *ChemPhysChem*, 2011, **12**, 2781-2785.
17. M. Valero, B. Zornoza, C. Tellez and J. Coronas, *Microporous Mesoporous Mater.*, 2014, **192**, 23-28.
18. H. Jeazet, S. Sorribas, J. Román-Marín, B. Zornoza, C. Téllez, J. Coronas and C. Janiak, *Eur. J. Inorg. Chem.*, 2016, 4363-4367.
19. M. Manttari, A. Pihlajamaki, E. Kaipainen and M. Nystrom, *Desalination*, 2002, **145**, 81-86.
20. R. R. Sharma, R. Agrawal and S. Chellam, *J. Membr. Sci.*, 2003, **223**, 69-87.
21. Y. He, G. M. Li, H. Wang, J. F. Zhao, H. X. Su and Q. Y. Huang, *J. Membr. Sci.*, 2008, **321**, 183-189.
22. T. Zhao, F. Jeremias, I. Boldog, B. Nguyen, S. K. Henninger and C. Janiak, *Dalton Trans.*, 2015, **44**, 16791-16801.
23. N. A. Khan, I. J. Kang, H. Y. Seok and S. H. Jhung, *Chem. Eng. J.*, 2011, **166**, 1152-1157.
24. J. Sanchez-Lainez, B. Zornoza, A. Mayoral, A. Berenguer-Murcia, D. Cazorla-Amoros, C. Tellez and J. Coronas, *J. Mater. Chem. A*, 2015, **3**, 6549-6556.
25. A. K. Ghosh and E. M. V. Hoek, *J. Membr. Sci.*, 2009, **336**, 140-148.
26. M. L. Lind, A. K. Ghosh, A. Jawor, X. F. Huang, W. Hou, Y. Yang and E. M. V. Hoek, *Langmuir*, 2009, **25**, 10139-10145.
27. G. Y. Chai and W. B. Krantz, *J. Membr. Sci.*, 1994, **93**, 175-192.
28. F. Cacho-Bailo, C. Tellez and J. Coronas, *Chem.-A Eur. J.*, 2016, **22**, 9533-9536.
29. R. Z. Jin, Z. Bian, J. Z. Li, M. X. Ding and L. X. Gao, *Dalton Trans.*, 2013, **42**, 3936-3940.
30. J. M. Zamaro, N. C. Perez, E. E. Miro, C. Casado, B. Seoane, C. Tellez and J. Coronas, *Chem. Eng. J.*, 2012, **195**, 180-187.
31. D. Y. Hong, Y. K. Hwang, C. Serre, G. Ferey and J. S. Chang, *Adv. Funct. Mater.*, 2009, **19**, 1537-1552.
32. J. Kim, S. Bhattacharjee, K. E. Jeong, S. Y. Jeong and W. S. Ahn, *Chem. Commun.*, 2009, 3904-3906.
33. S. K. Mohapatra, F. Hussain and P. Selvam, *Catal. Lett.*, 2003, **85**, 217-222.
34. C. M. Hansen, *Progr. Org. Coat.*, 2004, **51**, 77-84.
35. C. M. Hansen, *Eur. Polym. J.*, 2008, **44**, 2741-2748.
36. M. He, J. F. Yao, Q. Liu, Z. X. Zhong and H. T. Wang, *Dalton Trans.*, 2013, **42**, 16608-16613.
37. D. Fairen-Jimenez, S. A. Moggach, M. T. Wharmby, P. A. Wright, S. Parsons and T. Duren, *J. Am. Chem. Soc.*, 2011, **133**, 8900-8902.
38. N. Liedana, A. Galve, C. Rubio, C. Tellez and J. Coronas, *ACS Appl. Mater. Interfaces*, 2012, **4**, 5016-5021.
39. Y. Zhu, J. Ciston, B. Zheng, X. Miao, C. Czarnik, Y. Pan, R. Sougrat, Z. Lai, C.-E. Hslung, K. Yao, P. Ingo, M. Pan and Y. Han, *Nat. Mater.*, 2017, DOI: 10.1038/NMAT4852.
40. J. Coronas and J. Santamaria, *Sep. Purif. Methods*, 1999, **28**, 127-177.
41. W. X. Yao, K. J. Kennedy, C. M. Tam and J. D. Hazlett, *Can. J. Chem. Eng.*, 1994, **72**, 991-999.